Chapter 2
False Alarm in Satellite Precipitation Data

Evaluation of satellite precipitation algorithms is essential for future algorithm development. This is why many previous studies are devoted to the validation of satellite-based observations (e.g., Tian et al. 2009; Amitai et al. 2009; AghaKouchak et al. 2010b; Zhou 2008; Gochis et al. 2009; Yilmaz et al. 2005; Shen et al. 2010; Dinku et al. 2008; AghaKouchak et al. 2009; Liu et al. 2009; Sapiano and Arkin 2009; AghaKouchak et al. 2012). For instance, Tian et al. (2009) analyzed the error of six high-resolution satellite products versus a gauge-based estimate, and reported regional and seasonal variations of error patterns in the contiguous US. They conclude that satellite products tend to overestimate rainfall in the summer and underestimate it in the winter. Sapiano and Arkin (2009) also confirmed that satellites overestimate summertime convective storms over the US. Using Volumetric False Alarm Ratio, AghaKouchak et al. (2011) showed that several satellite products exhibit high false alarm rate for rainfall, especially at high quantiles of observation.

To investigate false alarms in satellite-based precipitation products, we conducted a validation study to compare PERSIANN and TRMM TB42 precipitation data with ground based measurements. False Alarm Ratio (FAR) and Probability of Detection (POD) are calculated for the time period between 2005 and 2008 over the US. The FAR is the ratio of falsely identified rainy pixels to the total number of rainy pixels in satellite data, whereas the POD measures the fraction of observed precipitation that was correctly forecasted (the ratio of the total number of times that rainfall was correctly forecasted to the total number of observed rainy pixels (Wilks 2006)). Figure 2.1 explains the definition of POD and FAR.

In the current study, the Stage IV radar-based multi-sensor precipitation estimates (MPE), available from the National Center for Environmental Prediction (NCEP), are used as the reference data. The Stage IV precipitation data are adjusted for various biases using rain gauge measurements (Lin and Mitchell 2005) and are considered the best area approximation among the currently available area-average rainfall datasets (AghaKouchak et al. 2010a; AghaKouchak et al. 2010c, d). Stage IV data is aggregated into 0.25 degree spatial and 3 hourly temporal resolutions, which is the same as the PERSIANN precipitation data. Figure 2.2 shows the FAR and POD for: (a) the entire period of 4 years, (b) the summer and (c) the winter

© Springer International Publishing Switzerland 2015

N. Nasrollahi, *Improving Infrared-Based Precipitation Retrieval Algorithms Using Multi-Spectral Satellite Imagery,* Springer Theses, DOI 10.1007/978-3-319-12081-2_2

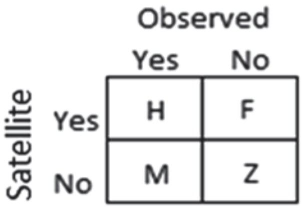

Fig. 2.1 The definition of Probability Of Detection (POD) and False Alarm Ratio (FAR)

seasons for the PERSIANN precipitation product (precipitation threshold is considered as 0.05 mm/h). Figure 2.2 reveals very high FARs over the central and western US and a lower FAR over the eastern US on average. Higher FAR is associated with presence of high cirrus clouds, especially in the winter. As discussed by Tian et al. (2009), PERSIANN data demonstrates higher FAR over the western US in the winter. The average POD is about 60 % over the central US and very low over the southwestern region. Low POD on the eastern and western side of the continent is associated with missed precipitation over these regions.

The missed precipitation may be caused by snow cover on the ground at higher latitudes or over the Rockies, and by the inability to catch warm rain processes or short-lived convective storms at lower latitudes, or maritime precipitation along the west coast (Tian et al. 2009).

Generally, probability of detection of satellite precipitation seems to be better during the summer seasons, perhaps due to a dominance of convective storms. On the other hand, the FAR is very high during the wintertime because of the presence of non-precipitating, high, cold clouds. Additionally, the presence of snow and ice on the ground and the inability of Passive Microwave (PMW) sensors to measure snowfall over snow or ice covered surfaces increase the error in satellite precipitation estimations and result in higher FARs during the wintertime. Figure 2.3 shows the same results for Tropical Rainfall Measuring Mission (TRMM) Multi-satellite Precipitation Analysis (TMPA) 3B42 precipitation data. Overall, both datasets show higher false rain during the winter and better estimations during summertime. Finally, it is worth mentioning that radar coverage is limited over the western region of the US (with the very high false alarm shown in Fig. 2.2 because of beam blockage in mountainous terrain). The Stage IV data has a large number of missing data over the Pacific Northwest region therefore, the precipitation data for this region is not included in the analysis.

In addition to calculation pixel-based false alarm, object-based approaches also show differences in precipitation estimations. For example, comparing different satellite-based precipitation patterns with the stage II radar-based precipitation pattern shows how the satellite estimations differ from radar observations. Figure 2.4 shows two satellite images that occurred at 0900 UTC 24 September 2005 during Hurricane Rita, with the spatial and temporal resolutions of 0.25×0.25 and 3 h [a: Tropical Rainfall Measuring Mission (TRMM) 3B42, Huffman et al. (2007); b: PERSIANN, Sorooshian et al. (2000)]. Hurricane Rita was one of the most intense tropical cyclones that made landfall on the U.S. Gulf Coast. Notice that in panels a to c, only precipitation values above the 50th percentile threshold are considered

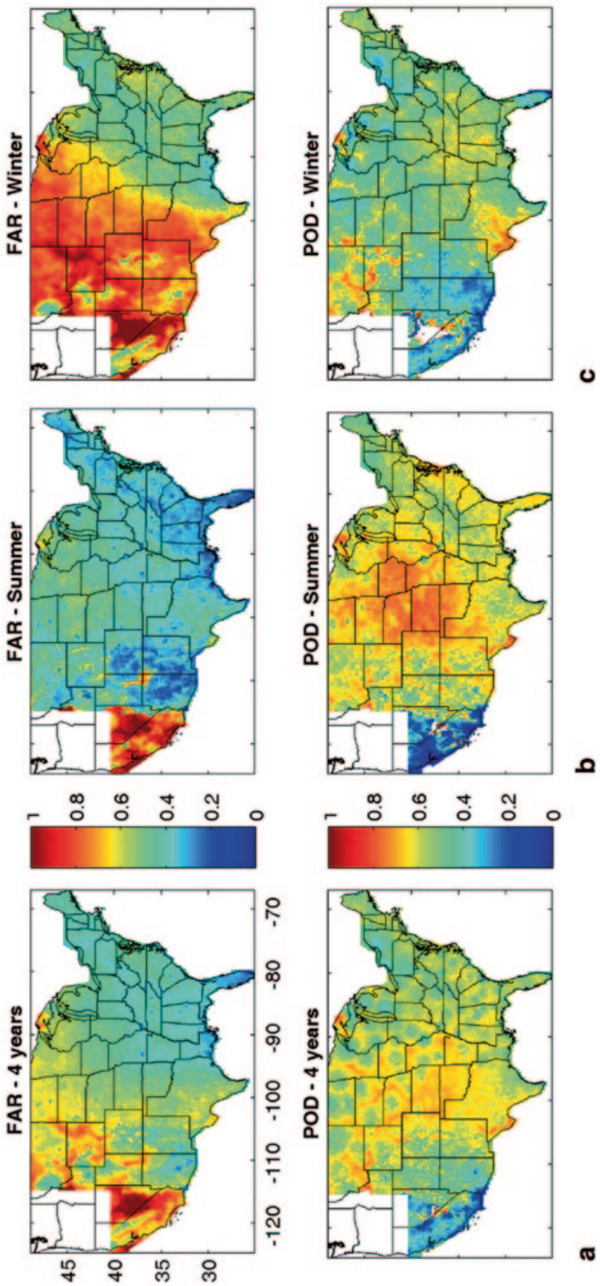

Fig. 2.2 False Alarm Ratio (*FAR*; *top three panels*) and Probability of Detection (*POD*; *bottom three panels*) of the PERSIANN precipitation data over the contiguous US (from 2005 to 2008). **a, d** 4 years results. **b, e** Summer season results. **c, f** Winter season results

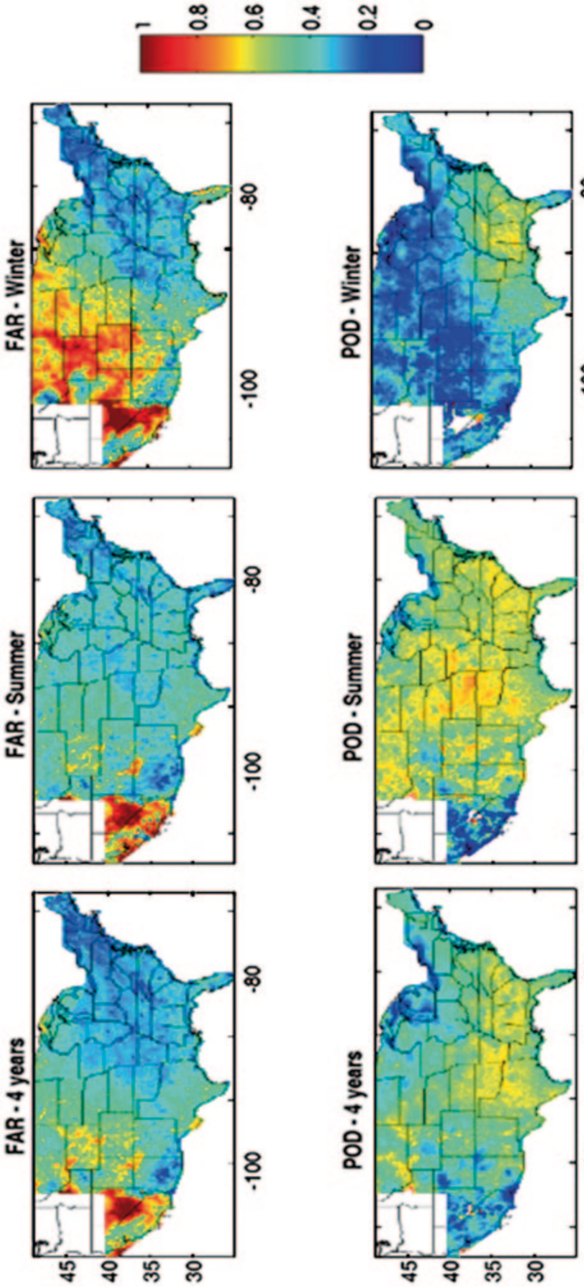

Fig. 2.3 False Alarm Ratio (*FAR*; *top three panels*) and Probability of Detection (*POD*; *bottom three panels*) of the TRMM 3B42 precipitation data over the contiguous US (from 2005 to 2008). **a, d** 4 years results. **b, e** Summer season results. **c, f** Winter season results

Fig. 2.4 The TRMM, PERSIANN and stage II precipitation pattern for rainfall rates above the 50th (**a–c**), 75th (**d–f**), 90th (**g–i**) percentiles

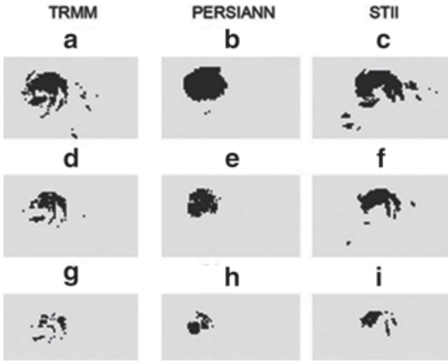

to avoid small rainfall rates. Panel c displays the corresponding stage II image. The stage II data provide estimates of precipitation using a combination of radar and rain gauge measurements. The data is available on the Hydrologic Rainfall Analysis Project (HRAP) grid, with a spatial resolution of approximately 4 km. The stage II data are aggregated in space to match the spatial resolution of TRMM and PERSIANN data. Panels d–f and g–i present similar figures for precipitation values exceeding the 75th and 90th percentiles, respectively. The domain of all figures includes 94×47 pixels, each being 0.25×0.25. With respect to the shape of patterns, the TRMM seem to be closer to the stage II data. However, for a higher threshold of 75th and 90th percentiles, the pattern of PERSIANN precipitation is more similar to those of stage II. It should be noted that the above example is provided to show differences in the pattern of precipitation and should not be considered as validation of satellite precipitation data.

References

AghaKouchak, A., Nasrollahi, N., & Habib, E. (2009). Accounting for Uncertainties of the TRMM Satellite Estimates, Remote Sensing, *1*(3), 606–619, doi:10.3390/rs1030606.

AghaKouchak, A., Bardossy, A., & Habib, E. (2010a). Copula-based uncertainty modeling: Application to multi-sensor precipitation estimates. *Hydrological Processes, 24*(15), 2111–2124.

AghaKouchak, A., Nasrollahi, N., Li, J., Imam, B., & Sorooshian, S. (2010b). Geometrical characterization of precipitation patterns. *Journal of Hydrometeorology, 12*(2), 274–285.

AghaKouchak, A., Habib, E., & Bardossy, A. (2010c). Modeling Radar Rainfall Estimation Uncertainties: Random Error Model, Journal of Hydrologic Engineering, *15*(4), 265–274, doi:10.1061/(ASCE)HE.1943-5584.0000185.

AghaKouchak, A., Bardossy, A., & Habib, E., (2010d). Conditional Simulation of Remotely Sensed Rainfall Fields Using a Non-Gaussian V-Transformed Copula, Advances in Water resources, *33*(6), 624–634, doi:10.1016/j.advwatres.2010.02.010.

AghaKouchak, A., Behrangi, A., Sorooshian, S., Hsu, K., & Amitai, E. (2011). Evaluation of satellite-retrieved extreme precipitation rates across the central United States. *Journal of Geophysical Research, 116,* D02115.

AghaKouchak, A., Mehran, A., Norouzi, H., & Behrangi, A. (2012). Systematic and random error components in satellite precipitation data sets. *Geophysical Research Letters, 39,* L09406.

Amitai, E., Llort, X., & Sempere-Torres, D. (2009). Comparison of TRMM radar rainfall estimates with NOAA next-generation QPE. *Journal of the Meteorological Society of Japan, 87,* 109–118.

Dinku, T., Chidzambwa, S., Ceccato, P., Connor, S., & Ropelewski, C. (2008). Validation of high-resolution satellite rainfall products over complex terrain. *International Journal of Remote Sensing, 29*(14), 4097–4110.

Gochis, D., Nesbitt, S., Yu, W., & Williams, S. (2009). Comparison of gauge-corrected versus non-gauge corrected satellite-based quantitative precipitation estimates during the 2004 name enhanced observing period. *Atmosfera, 22*(1), 69–98.

Huffman, G., Adler, R., Bolvin, D., Gu, G., Nelkin, E., Bowman, K., Stocker, E., & Wolff, D. (2007). The TRMM multi-satellite precipitation analysis: Quasi-global, multiyear, combined-sensor precipitation estimates at fine scale. *Journal of Hydrometeorology, 8,* 38–55.

Lin, Y., & Mitchell, K. E. (2005). The NCEP stage II/IV hourly precipitation analyses: Development and applications. Preprints, 19th Conf. on Hydrology, San Diego, CA, Am. Meteorol. Soc., 1.2.

Liu, Z., Rui, H., Teng, W., Chiu, L., Leptoukh, G., & Kempler, S. (2009). Developing an online information system prototype for global satellite precipitation algorithm validation and intercomparison. *Journal of Applied Meteorology and Climatology, 48*(12), 2581–2589.

Sapiano, M., & Arkin, P. (2009). An intercomparison and validation of high-resolution satellite precipitation estimates with 3-hourly gauge data. *Journal of Hydrometeorology, 10*(1), 149–166.

Shen, Y., Xiong, A., Wang, Y., & Xie, P. (2010). Performance of high-resolution satellite precipitation products over China. *Journal of Geophysical Research-Atmospheres, 115,* D02114.

Sorooshian, S., Hsu, K., Gao, X., Gupta, H., Imam, B., & Braithwaite, D. (2000). Evolution of the PERSIANN system satellite-based estimates of tropical rainfall. *Bulletin of the American Meteorological Society, 81*(9), 2035–2046.

Tian, Y., Peters-Lidard, C. D., Eylander, J. B., Joyce, R. J., Huffman, G. J., Adler, R. F., Hsu, K., Turk, F. J., Garcia, M., & Zeng, J. (2009). Component analysis of errors in satellite-based precipitation estimates, *Journal of Geophysical Research, 114,* D24101. doi:10.1029/2009JD011949.

Wilks, D. (2006). *Statistical methods in the atmospheric sciences*. (2nd ed., p. 627) Burlington: Academic

Yilmaz, K., Hogue, T., Hsu, K., Sorooshian, S., Gupta, H., & Wagener, T. (2005). Intercomparison of rain gauge, radar and satellite-based precipitation estimates with emphasis on hydrologic forecasting. *Journal of Hydrometeorology, 6*(4), 497–517.

Zhou, C., (2008). A two-step estimator of the extreme value index. *Extremes, 11*(3), 281–302.

http://www.springer.com/978-3-319-12080-5

Improving Infrared-Based Precipitation Retrieval
Algorithms Using Multi-Spectral Satellite Imagery
Nasrollahi, N.
2015, XXI, 68 p. 41 illus., 38 illus. in color., Hardcover
ISBN: 978-3-319-12080-5